GEOPHYSICS, VOL. 71, NO. 1 (JANUARY-FEBRUARY 2006); P. G1–G9, 7 FIGS., 2 TABLES.
10.1190/1.2168009

A 3D parametric inversion algorithm for triaxial induction data

Aria Abubakar[1], Tarek M. Habashy[1], Vladimir Druskin[1], Leonid Knizhnerman[2], and Sofia Davydycheva[3]

ABSTRACT

We develop a parametric inversion algorithm to determine simultaneously the horizontal and vertical resistivities of both the formation and invasion zones, invasion radius, bed boundary upper location and thickness, and relative dip angle from electromagnetic triaxial induction logging data. This is a full 3D inverse scattering problem in transversally isotropic media. To acquire sufficient sensitivity to invert for all of these parameters, we collect the data using a multicomponent, multispacing induction array. For each transmitter-receiver spacing this multicomponent tool has sets of three orthogonal transmitter and receiver coils. At each logging point single-frequency data are collected at multiple spacings to obtain information at different depths of investigation.

This inversion problem is solved iteratively with a constrained regularized Gauss-Newton minimization scheme. As documented in the literature, the main computational bottleneck when solving this full 3D inverse problem is the CPU time associated with constructing the Jacobian matrix. In this study, to achieve the inversion results within a reasonable computational time, we implement a dual grid approach wherein the Jacobian matrix is computed using a very coarse optimal grid. Furthermore, to regularize the inversion process we use the so-called multiplicative regularization technique. This technique automatically determines the regularization parameter.

Synthetic data tests indicate the developed inversion algorithm is robust in extracting formation and invasion anisotropic resistivities, invasion radii, bed boundary locations, relative dip, and azimuth angle from multispacing, multicomponent induction logging data.

INTRODUCTION

The anisotropic layered formation model with invasion for electrical resistivity (conductivity) is a useful model for interpreting oil- and gas-bearing reservoirs. For many sedimentary rocks, this resistivity anisotropy has a relative uniform value in the bedding plane (horizontal resistivity) and a varying value in the direction perpendicular to the plane (vertical resistivity). Such a medium is referred to as a transversally isotropic (TI) medium or TI anisotropic medium. A common case is a laminated sand-shale sequence where the horizontal resistivity is smaller than the vertical resistivity. In wells drilled perpendicular to bedding planes, conventional induction tools with vertical-component transmitters and receivers can only detect signals from currents that flow parallel to the bedding plane and hence cannot resolve the vertical resistivity. This greatly limits the application of these conventional tools and makes their interpretation unreliable in case if anisotropy is present.

A modern multicomponent induction tool that measures five components of magnetic fields has been developed by Kriegshauser et al. (2000). A fully multicomponent induction tool has also been developed by Rosthal et al. (2003) to measure all nine components of the magnetic fields. One of the main advantages of the latter tool is its ability to invert the relative azimuth angle by rotating the measurement tensor (without the need for any inversion procedure) as shown in Wang et al. (2003). Until now, most of the inversion algorithms developed for the multicomponent induction tool have been based on 1D models [neglecting the invasion zones; see Lu and Alumbaugh (2001), Yu et al. (2001), Wang et al. (2003), and Zhang et al. (2004)] or on 2D models [assuming the tool intersects the layering formation perpendicularly; see Zhang and Mezzatesta (2001)]. All of these assumptions can represent gross sources of error in the inversion procedure. Hence, a reliable quantitative interpretation of multicomponent, multispacing induction logging data can only be achieved by using

Manuscript received by the Editor December 2, 2004; revised manuscript received April 19, 2005; published online January 12, 2006; publisher error corrected January 17, 2006.
[1]Schlumberger-Doll Research, 36 Old Quarry Rd., Ridgefield, Connecticut 06810. E-mail: aabubakar@slb.com; thabashy@ridgefield.oilfield.slb.com; vdruskin@ridgefield.oilfield.slb.com.
[2]Central Geophysical Expedition, Narodnogo Opolcheniya St. 40-3, Moscow 123298, Russia. E-mail: mmd@cge.ru.
[3]Sugar Land Product Center, 110 Schlumberger Drive, MD5, Sugar Land, Texas 77478. E-mail: sdavydycheva@slb.com.

a full 3D inversion with features and capabilities that make it efficient and practical.

We propose a full 3D parametric inversion algorithm where we simultaneously invert the horizontal and vertical formation resistivities R_{th} and R_{tv}, the horizontal and vertical invasion resistivities R_{xoh} and R_{xov}, the invasion radii r, the bed boundary upper location z_1 and thickness Δz, and the relative dip angle θ after rotating the measurement data tensor to obtain the relative azimuth angle ϕ. The procedure to do this rotation is described in Wang et al. (2003). Note that the ability to rotate the data tensor is one of the significant advantages of a full multicomponent induction logging tool where the three orthogonal sensors are located at a common point.

Our inversion algorithm is a constrained, regularized Gauss-Newton minimization scheme (see Habashy and Abubakar, 2004). The forward simulator used to model the data is a fully anisotropic 3D finite-difference algorithm developed by Davydycheva et al. (2003). In the Gauss-Newton minimization scheme, the a priori information on the physical bounds of the unknown parameters is enforced using a nonlinear transformation. Furthermore, to guarantee an error-reducing minimization scheme, we use a line search and a backtracking procedure.

In this model-based inversion approach, the number of unknowns is less than the number of data points. Consequently, the Jacobian matrix is constructed by a direct finite difference obtained by a perturbation of the inverted parameters, one by one. For the example considered in our paper, the computational cost of such a Jacobian matrix construction is about 90% of the total computational time of the entire inversion procedure. To speed up the computation of the Jacobian matrix, we incorporated a very coarse optimal grid (see Druskin and Knizhnerman, 1999) for its calculation. Hence, in this inversion algorithm we introduce two different sets of optimal grids: a fine grid to calculate the cost functional to be minimized and a coarser grid to construct the Jacobian matrix. This approach significantly reduces the computational time, especially when the number of unknowns becomes large.

To improve the conditioning of our inversion algorithm, we use a multiplicative regularization analysis to determine the appropriate regularization parameter (see Abubakar et al., 2002). As a result of this analysis, the optimal regularization parameter is found to be proportional to the data misfit (the nonregularized cost functional). Hence, by using this particular choice of the regularization parameter, the characteristic of this inversion process is such that it will apply a large weighting parameter on the regularization term at the beginning of the optimization process when the data mismatch is large. In this case, the search direction is predominantly a steepest descent, which is the more appropriate approach to use in the initial steps of the optimization process since it tends to suppress large swings in the search direction. As the iteration proceeds, the optimization process gradually places more emphasis on minimizing the data mismatch and less emphasis on the regularization term. In this case, the search direction corresponds to a Newton search method, which is the more appropriate approach to use as we get closer to the minimum of the nonregularized cost functional where the quadratic model for the cost functional becomes more accurate. Furthermore, if noise is present in the data, the data misfit generally will be bounded below by the level of noise present. Hence, the weight of the regularization term is adjusted in an adaptive fashion so as not to fall below the noise level. This suppresses any magnification of the noise as a result of the presence of small eigenvalues in the spectrum of the inversion operator. This feature is extremely important when we have measurements that are redundant or lack sensitivity to certain model parameters resulting from the poor conditioning of the inversion.

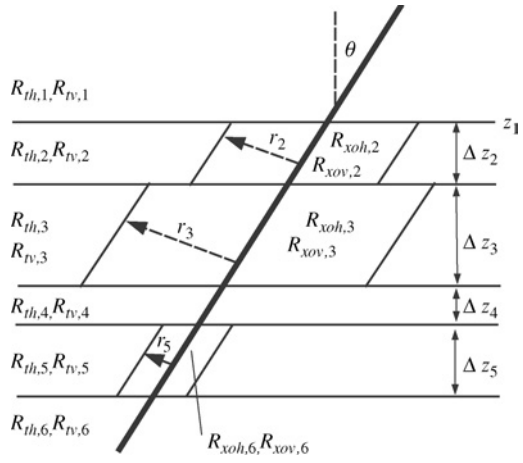

Figure 1. Parametric model used in the inversion algorithm.

INVERSION ALGORITHM

Here, we adopt a model-based inversion approach. Our generic model is a dipping TI anisotropic layered formation with a pistonlike invasion. Figure 1 shows a six-layer example for such a formation model. The ith layer is characterized by its horizontal and vertical formation resistivities ($R_{th,i}$, $R_{tv,i}$), horizontal and vertical invasion resistivities ($R_{xoh,i}$, $R_{xov,i}$), invasion radius r_i, and the layer thickness Δz_i. In addition to these model parameters per layer, we also have parameters that define the overall formation model. These are the location of the uppermost bed boundary z_1, the relative dip angle θ, and the relative azimuth angle ϕ. This leads to a total of $6B + 1$ parameters for a formation that has B layers. No borehole parameters are included in the inversion since the measurements are assumed to be borehole corrected.

The data used in the inversion are collected using a tool that consists of three orthogonal transmitters, all located at the same position on the tool axis, and three orthogonal receivers similarly arranged. Hence, for each transmitter-receiver spacing this multicomponent, multispacing tool measures all nine components of the magnetic field: H_{xx}, H_{xy}, H_{xz}, H_{yx}, H_{yy}, H_{yz}, H_{zx}, H_{zy}, and H_{zz}. The symbol H_{ij} denotes the magnetic field recorded by the j receiver from the i-transmitter. For a TI anisotropic formation with dip but no strike, i.e., with an azimuth angle $\phi = 0$, the magnetic field components H_{xy}, H_{yx}, H_{yz}, and H_{zy} vanish. Hence, the azimuth angle ϕ is reconstructed first by estimating the azimuth angle at which the data tensor can be rotated to minimize the cross-coupling components of the magnetic field (H_{xy}, H_{yx}, H_{yz}, and H_{zy}) for each transmitter-receiver spacing. This is done in a least-squares sense. Such a rotation places the y-axis of our model along the relative strike of the formation. As indicated by Zhang et al. (2004), this procedure of resolving

ϕ without carrying out an inversion is only possible when all magnetic-field components for each transmitter-receiver spacing are measured at the same position.

After resolving the azimuthal angle, a total of $N = 6B$ model parameters must be inverted. These parameters are assembled in the model parameter vector $\mathbf{x}$ defined by

$$\mathbf{x} = [R_{th,1}, R_{tv,1}, R_{xoh,1}, R_{xov,1}, \ldots, R_{xoh,B}, R_{xov,B}, r_1, r_2, \cdots, r_B, z_1, \Delta z_2, \ldots, \Delta z_{B-1}, \theta]^T, \quad (1)$$

where the superscript T indicates transposition.

The measurement data is assembled in a vector $\mathbf{m}$ defined by

$$\mathbf{m} = [\mathrm{Im}(H_{xx,1}), \mathrm{Im}(H_{xz,1}), \mathrm{Im}(H_{yy,1}), \mathrm{Im}(H_{zx,1}), \mathrm{Im}(H_{zz,1}), \ldots, \mathrm{Im}(H_{zz,L\times R})]^T, \quad (2)$$

where $L \times R$ is the number of logging points times the number of receiver arrays. Hence, in total we have $M = 5L \times R$ corresponding to the five self- and cross-coupling components of the magnetic field. Note that in equation 2 we only include the imaginary part of the magnetic field in the inversion, since it is the dominant part of the complex field resulting from the presence of the inhomogeneity in the formation.

The unknown model parameter $\mathbf{x}$ is updated iteratively by minimizing a quadratic cost functional of the form

$$C(\mathbf{x}) = \frac{1}{2}\left[\|\mathbf{W}_d \cdot \mathbf{r}(\mathbf{x})\|^2 + \lambda\|\mathbf{W}_x \cdot (\mathbf{x} - \mathbf{x}_{\mathrm{ref}})\|^2\right], \quad (3)$$

where $\|\cdot\|$ denotes the L_2-norm of a vector and $\mathbf{r}$ is the residual error defined as

$$r_j(\mathbf{x}) = s_j(\mathbf{x}) - m_j, \qquad j = 1, 2, \ldots, M, \quad (4)$$

in which $\mathbf{s}(\mathbf{x})$ is the simulated tool response corresponding to a particular value of the model parameter $\mathbf{x}$. The positive scalar factor λ in equation 3 is the regularization parameter. It is a trade-off parameter determining the relative importance of the two terms in the cost functional. The first term in the cost functional represents the misfit between the measured and predicted responses, the so-called data misfit. The second term is included to regularize the optimization problem. The value $\mathbf{W}_x^T \cdot \mathbf{W}_x$ is the inverse of the model covariance matrix, representing the degree of confidence in the reference model $\mathbf{x}_{\mathrm{ref}}$ and provided as a priori information. The value $\mathbf{W}_d^T \cdot \mathbf{W}_d$ is the inverse of the data covariance matrix, which describes the estimated uncertainties from noise contamination in the available data set. It describes not only the estimated variance for each particular data point but also the estimated correlation between errors. It therefore provides point-by-point weighting of the input data according to a prescribed criterion.

To solve equation 3, we use a Gauss-Newton minimization approach, which approximates a nonlinear function with a local quadratic model constructed from the knowledge of the first derivative evaluated at the current iterate. The Gauss-Newton minimization approach has an overall convergence rate that is slightly less than quadratic but significantly better than linear. It also provides quadratic convergence in a neighborhood of the minimum. We also incorporate a line search along the Gauss-Newton step direction to guarantee a reduced cost functional after each iteration.

The unknown model parameter is updated from iterate k to iterate $k + 1$ as follows:

$$\mathbf{x}_{k+1} = \mathbf{x}_k + \nu_k \mathbf{p}_k, \quad (5)$$

where ν_k is a positive real number chosen by means of the line search procedure and $\mathbf{p}_k$ is the Gauss-Newton step given by

$$\mathbf{p}_k = -\mathbf{H}_k^{-1} \cdot \mathbf{g}_k, \quad (6)$$

in which the gradient $\mathbf{g}_k$ and the Hessian matrix $\mathbf{H}_k$ are given by

$$\mathbf{g}_k = \nabla C(\mathbf{x})|_{\mathbf{x}=\mathbf{x}_k} = \mathbf{J}_k^T \cdot \mathbf{W}_d^T \cdot \mathbf{W}_d \cdot \mathbf{r}_k + \lambda \mathbf{W}_x^T \cdot \mathbf{W}_x \cdot (\mathbf{x}_k - \mathbf{x}_{\mathrm{ref}}) \quad (7)$$

and

$$\mathbf{H}_k = \nabla\nabla C(\mathbf{x})|_{\mathbf{x}=\mathbf{x}_k} = \mathbf{J}_k^T \cdot \mathbf{W}_d^T \cdot \mathbf{W}_d \cdot \mathbf{J}_k + \lambda \mathbf{W}_x^T \cdot \mathbf{W}_x. \quad (8)$$

In equation 8 we neglect second-order derivatives in the Hessian matrix. Since in this model-based inversion the total number of unknowns is not enormously large, the Hessian matrix $\mathbf{H}_k$ is inverted using a simple Gaussian elimination procedure (see Press et al., 1992). In equations 7 and 8 the Jacobian matrix $\mathbf{J}(\mathbf{x})$ is given by

$$\mathbf{J}(\mathbf{x}) = \begin{bmatrix} \partial s_1/\partial x_1 & \ldots & \partial s_1/\partial x_i & \ldots & \partial s_1/\partial x_N \\ \vdots & \ddots & \vdots & \ddots & \vdots \\ \partial s_j/\partial x_1 & \ldots & \partial s_j/\partial x_i & \ldots & \partial s_j/\partial x_N \\ \vdots & \ddots & \vdots & \ddots & \vdots \\ \partial s_M/\partial x_1 & \ldots & \partial s_M/\partial x_i & \ldots & \partial s_M/\partial x_N \end{bmatrix}, \quad (9)$$

where each entry of the Jacobian matrix is estimated through a finite-difference computation,

$$\frac{\partial s_j(\mathbf{x})}{\partial x_i} \approx \frac{s_j[(1+\Delta)x_i] - s_j(x_i)}{\Delta x_i}. \quad (10)$$

In our implementation Δ is taken to be equal to 10^{-4}. As is clear from equation 10, the computation of this Jacobian matrix $\mathbf{J}(\mathbf{x})$ will dominate the total computation time of the inversion procedure. In each Gauss-Newton step we need to solve $M \times N$ forward problems to construct $\mathbf{J}(\mathbf{x})$.

Computing the Jacobian matrix

To obtain the inversion results within acceptable computation time, we calculate each entry of the Jacobian matrix approximately, i.e.,

$$\frac{\partial s_j(\mathbf{x})}{\partial x_i} \approx \frac{s_j^{\mathrm{app}}[(1+\Delta)x_i] - s_j^{\mathrm{app}}(x_i)}{\Delta x_i}. \quad (11)$$

This approximate solution $\mathbf{s}^{\mathrm{app}}(\mathbf{x})$ is calculated using the finite-difference forward-modeling code on a coarse optimal grid along both the radial direction (the x-direction) and the invariant direction (the y-direction). Druskin and Knizhnerman (1999) show this optimal grid results in finite-difference schemes that are exponentially convergent. In this study, we

use only three nodes on the optimal grid in the x- and y-directions to calculate $\mathbf{s}^{\text{app}}(\mathbf{x})$.

To illustrate the effect of coarsening the optimal grid in the forward-modeling code, we show in Figure 2 the forward-modeling responses of the uninvaded nine-layer TI anisotropic with dip model given in Wang et al. (2003). The values of the formation resistivity and the bed-boundary parameters of this model are given in Table 1. In Figure 2 we present the imaginary part of the xx- and zx-components of the simulated magnetic field and compare it with the simulated magnetic field generated by a semianalytical forward code. The transmitter-receiver spacing used in calculating the responses shown in Figure 2 is 1.827 m and the frequency of operation is 20 kHz. The computation times of our forward code for one logging point, for all six receiver arrays (varied from 0.3045 m up to 1.827 m), and for each transmitter polarization are about 0.5 s (for three nodes), 4 s (for five nodes), and 17 s (for seven nodes) on a PC with a Pentium IV 2.4-GHz processor. Thus, by using an approximate Jacobian matrix calculated by a minimum number of the optimal grid, we can significantly reduce the computation. When we use the grid set with five nodes for computing the data mismatch and the grid set with three nodes for computing the Jacobian, the reduction in computation time will be at least a factor of eight.

Table 1. Model parameters of the noninvaded nine-layer TI anisotropic with dip model; $z_1 = 3.045$ ft and $\theta = 60°$.

Δz (tvd in m)	R_{th} (Ω-m)	R_{tv} (Ω-m)
	10	10
2.436	50	200
2.436	10	10
1.218	50	200
1.218	10	10
1.218	0.5	2
2.436	10	10
2.436	0.5	2
	10	10

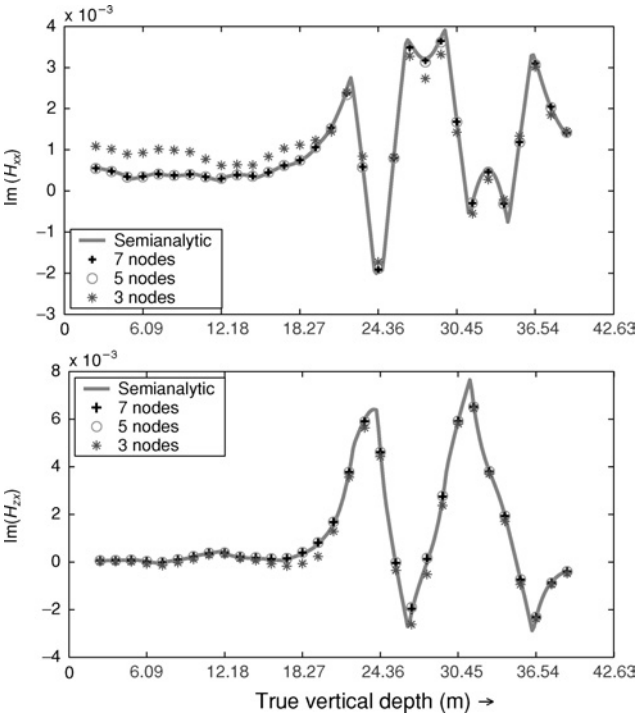

Figure 2. Comparison of the uninvaded nine-layer TI anisotropic with dip model responses between a semianalytical code and our forward code using different number of discretization nodes in the x- and y-directions.

More details about the effect of reducing the number of optimal grids in our forward simulator can be found in Davydycheva et al. (2003). Furthermore, a similar strategy is used by Kriegshauser et al. (2001) to solve a 2D problem for multicomponent induction logging data. In their work they use a 1D forward model to estimate the Jacobian matrix, showing that the difference of the eigenvalues of the exact and the approximate Jacobian is within an acceptable level. The effectiveness of using a coarse grid to compute the Jacobian matrix is borne out by the successful inversion carried out in the numerical examples section below.

Line-search procedure

An important feature of the inversion scheme is imposing a line-search procedure along the descent direction that guarantees a reduction in the cost functional in equation 3 after each iteration. This is done by calculating a scalar real positive parameter ν_k that minimizes the cost functional $C(\mathbf{x}_k + \nu_k \mathbf{p}_k)$. Since ν_k is a scalar quantity, this minimization can in principle be carried out by using any simple nonlinear minimization routine (see Press et al., 1992). However, if the evaluation of the cost function of equation 3 (which translates to calculating the forward model) is expensive, as in this case, a full nonlinear determination of ν_k might not be efficient from a computational-cost viewpoint. It is therefore desirable to limit the number of such evaluations as much as possible.

To do so, we adopt a procedure (see Dennis and Schnabel, 1983) whereby a step-length ν_k is selected to reduce the cost functional such that the average rate of decrease from $C(\mathbf{x}_k)$ to $C(\mathbf{x}_k + \nu_k \mathbf{p}_k)$ is at least some prescribed fraction α of the initial rate of decrease at $\mathbf{x}_k$ along the direction $\mathbf{p}_k$, i.e.,

$$C(\mathbf{x}_k + \nu_k \mathbf{p}_k) \leq C(\mathbf{x}_k) + \alpha \nu_k \delta C_{k+1}. \tag{12}$$

In equation 12, $0 < \alpha < 1$ is a fractional number that, in practice, is set quite small (we set α to 10^{-4}) so that little more than a decrease in the cost functional value is required. The symbol δC_{k+1} denotes the rate of decrease of $C(\mathbf{x})$ at $\mathbf{x}_k$ along the direction $\mathbf{p}_k$ and is given by

$$\delta C_{k+1} = \frac{\partial}{\partial \nu} C(\mathbf{x}_k + \nu \mathbf{p}_k)\bigg|_{\nu=0} = \mathbf{g}^T(\mathbf{x}_k) \cdot \mathbf{p}_k. \tag{13}$$

The procedure we adopt is to first use the full Gauss-Newton search step. If $\nu_k = 1$ fails to satisfy the criterion given by equation 12, we then backtrack along the direction of the Gauss-Newton step until an acceptable next iterate according to equation 5 is found. If, at the $(k+1)$th iteration, $\nu_k^{(m)}$ is the current mth step-length that does not satisfy the condition of equation 12, we compute the next backtracking step-length $\nu_k^{(m+1)}$ by searching for the minimum of the cost functional, assuming a quadratic approximation:

$$f(\nu) \equiv C(\mathbf{x}_k + \nu \mathbf{p}_k) \approx a + b\nu + c\nu^2, \tag{14}$$

where the real constants a, b, and c are determined from the current information on the cost functional $C(\mathbf{x})$. Thus, $\nu_k^{(m+1)}$, which is the minimum of $f(\nu)$, for $m = 0, 1, 2, \ldots$ is given by

$$\nu_k^{(m+1)} = -\frac{b}{2c} = -\frac{1}{2}\frac{\left[\nu_k^{(m)}\right]^2 \delta C_{k+1}}{C\left(\mathbf{x}_k + \nu_k^{(m)}\mathbf{p}_k\right) - C(\mathbf{x}_k) - \nu_k^{(m)}\delta C_{k+1}}. \quad (15)$$

We start with $\nu_k^{(0)} = 1$ (full Gauss-Newton step) and proceed with the backtracking procedure of equation 15 until condition 12 is satisfied. In general, it is not desirable to decrease $\nu_k^{(m+1)}$ too much since this may excessively slow the iterative process. To prevent this slowdown, we set $\nu_k^{(m+1)} = 0.1\nu_k^{(m)}$ if $\nu_k^{(m+1)} < 0.1\nu_k^{(m)}$ (but with ν_k not to drop below 0.1, i.e., $\nu_k^{\min} = 0.1$, to guard against too small a value of ν) and then proceed with the iteration.

Constraining the inversion process

To impose a priori information such as positivity or maximum and minimum bounds on the unknown model parameters, $\mathbf{x} = [x_i, i = 1, 2, \ldots, N]$, we introduce a nonlinear transformation of the form

$$x_i = \frac{x_i^{\max} + x_i^{\min}}{2} + \frac{x_i^{\max} - x_i^{\min}}{2}\sin(c_i), \quad -\infty < c_i < \infty, \quad (16)$$

where $x_i^{\max}$ and $x_i^{\min}$ are the upper and lower bounds on the physical model parameter x_i. It is clear that

$$x_i \to x_i^{\min}, \quad \text{as} \quad \sin(c_i) \to -1, \quad (17)$$

$$x_i \to x_i^{\max}, \quad \text{as} \quad \sin(c_i) \to +1. \quad (18)$$

These nonlinear transformations force the reconstruction of the model parameters to lie always within their physical bounds. Formally by using this nonlinear transformation we should update the artificial unknown parameters c_i instead of the physical model parameters x_i. However, it is straightforward to show that

$$\frac{\partial s_j}{\partial c_i} = \frac{dx_i}{dc_i}\frac{\partial s_j}{\partial x_i} = \sqrt{\left(x_i^{\max} - x_i\right)\left(x_i - x_i^{\min}\right)}\frac{\partial s_j}{\partial x_i}. \quad (19)$$

The two successive iterates $x_{i,k+1}$ and $x_{i,k}$ of x_i are related by

$$x_{i,k+1} = \frac{x_i^{\max} + x_i^{\min}}{2} + \frac{x_i^{\max} - x_i^{\min}}{2}\sin(c_{i,k+1}) = \frac{x_i^{\max} + x_i^{\min}}{2} + \frac{x_i^{\max} - x_i^{\min}}{2}\sin(c_{i,k} + q_{i,k}), \quad (20)$$

where

$$c_{i,k} = \arcsin\left(\frac{2x_{i,k} - x_i^{\max} - x_i^{\min}}{x_i^{\max} - x_i^{\min}}\right), \quad (21)$$

and where $q_{i,k} = c_{i,k+1} - c_{i,k}$ is the Gauss-Newton search step in c_i toward the minimum of the cost functional in equation 3. This Gauss-Newton direction in c_i is related to the Gauss-Newton direction in x_i through the following relation:

$$p_i = q_i\frac{\mathrm{d}x_i}{\mathrm{d}c_i}. \quad (22)$$

Hence, by using the relationship of equation 22 in equation 20, we obtain the following relationship between the two successive iterates $x_{i,k+1}$ and $x_{i,k}$ of x_i (assuming an adjustable steplength ν_k along the search direction x_i):

$$x_{i,k+1} = \frac{x_i^{\max} + x_i^{\min}}{2} + \left(x_{i,k} - \frac{x_i^{\max} + x_i^{\min}}{2}\right)\cos\left(\frac{\nu_k p_{i,k}}{\gamma_k}\right) + \gamma_k \sin\left(\frac{\nu_k p_{i,k}}{\gamma_k}\right), \quad (23)$$

where

$$\gamma_k = \sqrt{\left(x_i^{\max} - x_{i,k}\right)\left(x_{i,k} - x_i^{\min}\right)}. \quad (24)$$

Thus, in the inversion process there is no need to compute either c_i or q_i explicitly. This will reduce the round-off errors caused by introducing of the nonlinear function.

Choosing the regularization parameter

Another important ingredient of any optimization method is to determine the regularization parameter λ in the cost functional $C(\mathbf{x})$. Abubakar et al. (2003) introduce an automated way to adaptively choose the regularization parameter. In this approach the regularization is introduced as a multiplicative factor in the cost functional. As a result of the analysis in Habashy and Abubakar (2004), the regularization parameter is found to be proportional to the nonregularized cost functional, i.e., the first term of the cost function defined in equation 3. Together with a conjugate-gradient algorithm, this regularization technique is effective in inverting synthetic and experimental data [see Abubakar et al. (2003) and van den Berg et al. (2003)]. We adapt this multiplicative regularization technique with a Newton-type algorithm. To that end, we modify the cost functional given in equation 3 as follows:

$$C_k(\mathbf{x}) = F(\mathbf{x})R_k(\mathbf{x}), \quad (25)$$

where $F(\mathbf{x})$ is the cost functional corresponding to the data mismatch

$$F(\mathbf{x}) = \frac{1}{2}\|\mathbf{W}_d \cdot \mathbf{r}(\mathbf{x})\|^2 \quad (26)$$

and $R_k(\mathbf{x})$ is the regularization factor, chosen to be

$$R_k(\mathbf{x}) = \eta_k(\|\mathbf{W}_x \cdot (\mathbf{x} - \mathbf{x}_{\text{ref}})\|^2 + \|\delta\|^2), \quad (27)$$

where

$$\eta_k = \frac{1}{\|\mathbf{W}_x \cdot (\mathbf{x}_k - \mathbf{x}_{\text{ref}})\|^2 + \|\delta\|^2}, \quad (28)$$

in which δ is a constant parameter to be determined by numerical experimentation. One should note that the regularization process is far less sensitive to the parameter δ than to the Tikhonov regularization parameter λ. For all of our examples, we only use one value for δ. The normalization η_k in the regularization factor $R_k(\mathbf{x})$ is chosen so that $R_k(\mathbf{x} = \mathbf{x}_k) = 1$. This means that at the end of the optimization process the value of the regularization parameter will be close to unity, i.e.,

$$\lim_{k\to\infty} R_k(\mathbf{x}_{k+1}) = 1. \quad (29)$$

The gradient of the cost functional $C_k(\mathbf{x})$ in equation 25 is given by

$$\mathbf{g}_k = \mathbf{J}_k^T \cdot \mathbf{W}_d^T \cdot \mathbf{W}_d \cdot \mathbf{r}_k + \eta_k F(\mathbf{x}_k)\mathbf{W}_x^T \cdot \mathbf{W}_x \cdot (\mathbf{x}_k - \mathbf{x}_{\text{ref}}), \tag{30}$$

and its Hessian matrix is given by

$$\begin{aligned}\mathbf{H}_k = {} & \mathbf{J}_k^T \cdot \mathbf{W}_d^T \cdot \mathbf{W}_d \cdot \mathbf{J}_k + \eta_k F(\mathbf{x}_k)\mathbf{W}_x^T \cdot \mathbf{W}_x \\ & + \eta_k \left[\mathbf{W}_x^T \cdot \mathbf{W}_x \cdot (\mathbf{x}_k - \mathbf{x}_{\text{ref}})\right]^T \cdot \mathbf{J}_k^T \cdot \mathbf{W}_d^T \cdot \mathbf{W}_d \cdot \mathbf{r}_k \\ & + \eta_k \left[\mathbf{J}_k^T \cdot \mathbf{W}_d^T \cdot \mathbf{W}_d \cdot \mathbf{r}_k\right]^T \cdot \mathbf{W}_x^T \cdot \mathbf{W}_x \cdot (\mathbf{x}_k - \mathbf{x}_{\text{ref}}).\end{aligned} \tag{31}$$

In our numerical implementation and to restrain the inversion process from exhibiting huge jumps between two successive iterations, we set $\mathbf{x}_{\text{ref}}$ to be the value of $\mathbf{x}$ at the previous iteration. For this particular choice of $\mathbf{x}_{\text{ref}}$, the multiplicative cost functional in equation 25 is equivalent to the additive one in equation 3 if we choose λ to vary according to

$$\lambda_k = \frac{F(\mathbf{x}_k)}{\|\delta\|^4}. \tag{32}$$

By using the value of the regularization parameter given in equation 32, our minimization procedure will place a relatively large weight on the regularization term at the beginning of the inversion process, when the value of the data misfit $F(\mathbf{x})$ is still large. In this case, the search direction is predominantly a steepest descent, which is the more appropriate approach to use during the initial steps of the iteration since it has the tendency of suppressing large swings in the search direction. As the iteration proceeds, less weight is put on the regularization term of the cost functional, hence minimizing the data mismatch of the cost functional. In this case the search direction corresponds to a Newton search method, which is the more appropriate approach to use as we get closer to the minimum of the cost functional $F(\mathbf{x})$ where the quadratic approximation becomes more accurate.

If noise is present in the data, the data misfit term will have a minimum value determined by the noise level present in the data. As a consequence, the regularization term will be large enough to suppress the effect of the noise on the inversion process.

Finally, we note that the main advantage of using the procedure described above is that the inversion process automatically and adaptively determines the regularization parameter.

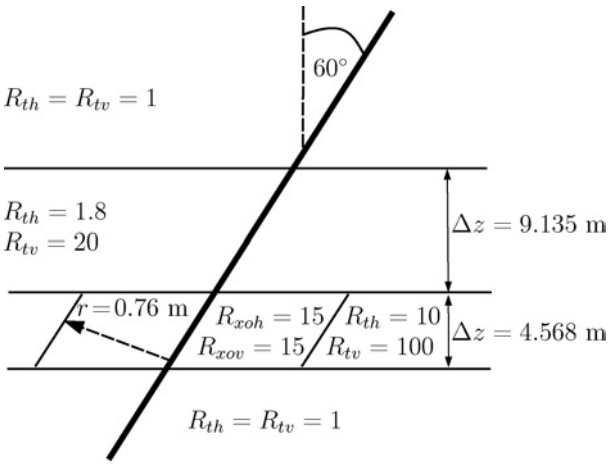

Figure 3. A dipping-bed model derived from a measured log in Egypt. The resistivities are in ohm-m.

Stopping criterion

The inversion process is terminated when either the relative data misfit reaches a prescribed value, the number of iteration exceeds the prescribed maximum, the differences between two successive iterates of the model parameters, or the cost function is within a prescribed tolerance factor. More details about the stopping criterion can be found in Habashy and Abubakar (2004).

NUMERICAL EXAMPLES

We now apply our inversion algorithm to synthetic data sets. In the inversion process the resistivity, invasion radius, dip angle, and the bed-boundary parameters are enforced to lie within the following bounds:

$$\begin{aligned} 10^{-4}\,\text{ohm-m} < R_i < 10^4\,\text{ohm-m}, \\ 2.358 \times 10^{-3}\,\text{m} < r_i < 2.030\,\text{m}, \\ 3.045 \times 10^{-2}\,\text{m} < z_1 < 12.180\,\text{m}, \\ 3.045 \times 10^{-2}\,\text{m} < \Delta z_i < 24.360\,\text{m}, \\ 0.1^\circ < \theta < 90^\circ \end{aligned} \tag{33}$$

by using the nonlinear transformation procedure. The covariance matrix $\mathbf{W}_d$ is chosen to be

$$\mathbf{W}_d = \frac{1}{\|\mathbf{m}\|}\mathbf{I}, \tag{34}$$

where $\mathbf{I}$ is the identity matrix. We note that a different covariance matrix $\mathbf{W}_d$ could boost the sensitivity of the data with respect to some particular parameters. The construction of such matrices is beyond the scope of this study. Moreover, we use the simplest covariance matrix, since our objective is to test the inversion algorithm in the worst-case scenario. The covariance matrix $\mathbf{W}_x$ is chosen to be

$$\mathbf{W}_x = \begin{bmatrix} \frac{1}{x_{\text{ref},1}} & \cdots & 0 & \cdots & 0 \\ \vdots & \ddots & \vdots & \ddots & \vdots \\ 0 & \cdots & \frac{1}{x_{\text{ref},\frac{N}{2}}} & \cdots & 0 \\ \vdots & \ddots & \vdots & \ddots & \vdots \\ 0 & \cdots & 0 & \cdots & \frac{1}{x_{\text{ref},N}} \end{bmatrix}, \tag{35}$$

with $x_{\text{ref},i} \neq 0$ for $i = 1, 2, \cdots, N$. Note that the use of equation 35 is necessary since we are dealing with inverting of model parameters with different physical dimensions.

For the first example we consider a dipping-bed formation model as shown in Figure 3. This formation model was derived from a measured log in a field in Egypt. The formation is characterized by a low-resistivity pay zone above an invaded pay sand. The dip angle is 60°.

The measured data used in the inversion are sampled every 2.436 m starting from 3.045 m up to 37.149 m in measured depth (corresponding to 15 logging points). At each logging point we collect the data using six receiver arrays. The frequency of operation is 20 kHz. The details of the triaxial tool arrays are given in Barber et al. (2004). After rotating the tensor measurement data along the strike, the total independent data points add up to 450 points.

As an initial guess for starting the inversion, we use a homogeneous whole-space model of 10 ohm-m resistivity. The initial guess for the dip angle is 20°. In the inversion we fix the number of layers to four. This is the only a priori information that introduced in our inversion procedure. In Figure 4 we present the 1D plots of the true, initial, and inverted model parameters of the dipping-bed model given in Figure 3 as a function of the measured depth. The true model parameters are given by the solid lines, while the initial and inverted model parameters are given by the green-dashed and blue-dashed-dotted lines, respectively. The horizontal and vertical formation resistivities are given by the top plots, the horizontal and vertical invasion resistivities are given by the middle plots, and the invasion radii (in inches) are given by the bottom plot. The inversion process is terminated when the value of $\sqrt{F(\mathbf{x}_k)}$ given in equation 26 reaches the level of 0.01%. In this case of noise-free data, we obviously obtain an excellent reconstruction results, as shown in Figure 3.

Next, we add 5% random white noise to all of the data. The corresponding inversion results are shown in Figure 5. The inversion process is terminated after the data misfit reaches

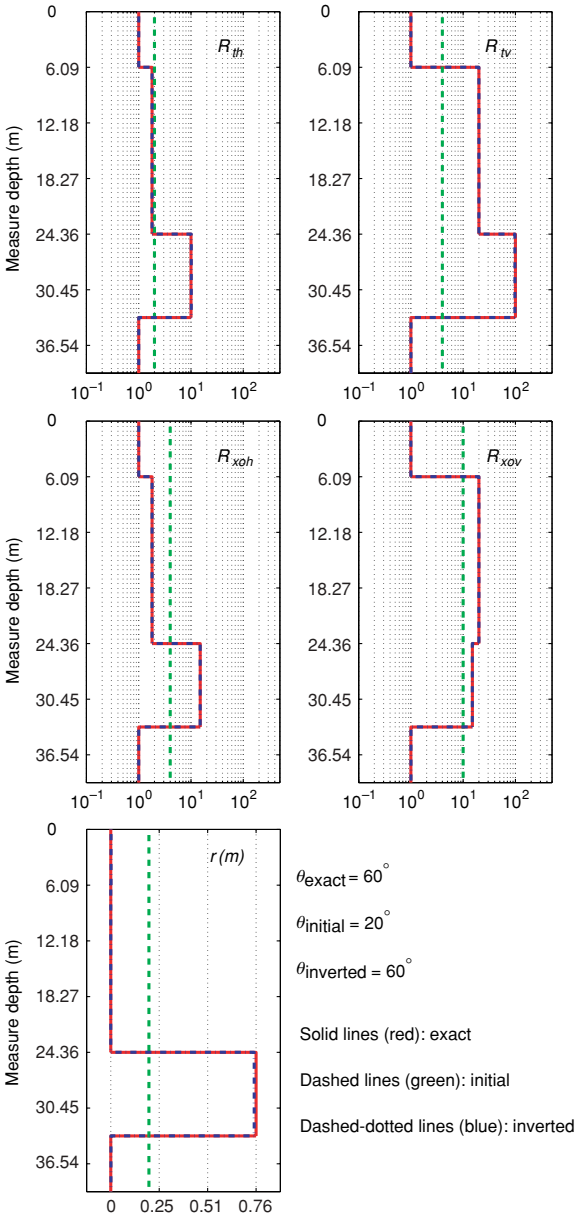

Figure 4. The inversion results of the dipping-bed model given in Figure 3 using clean data collected at 15 logging points.

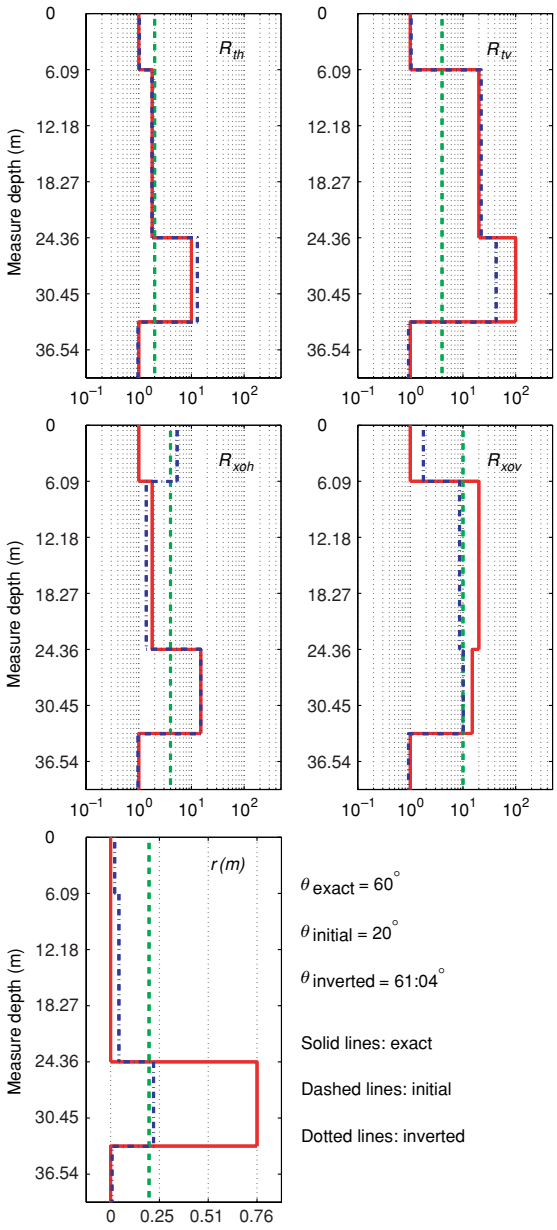

Figure 5. The inversion results of the dipping-bed model given in Figure 3 using data with 5% random white noise collected at 15 logging points.

a value of 3.4%. Note that the inversion does a better job 10b in inverting the bed-boundary parameters and dip angle than in inverting the formation and invasion resistivities. This indicates the multicomponent, multispace induction logging data have more than adequate sensitivity to invert these geometrical parameters.

To improve the reconstruction results, we add more data in the inversion process. The measured data are collected every 1.218 m, starting from 3.045 m up to 37.149 m in measured depth (corresponding to 29 logging points). To this data set, we again add 5% random white noise. The inversion results using this data set are given in Figure 6. As shown in Figure 6, the reconstruction results are significantly improved. The final data misfit of the inversion using this data set is approximately 3.5%.

In the second example we consider a nine-layer formation with dip and invasion. This formation consists of several high- and low-resistivity layers. The dip angle in this formation is 60°. The true model parameters are given in Table 2. The data are collected using 69 logging points starting from $z = 0$ up to $z = 41.412$ m in measured depth. The total number of data points is 2070. A 5% random white noise is added to the data used in the inversion. As an initial guess for the inversion, we use a homogeneous whole-space model of 10 ohm-m resistivity.

The inversion process terminates after 25 iterations. The inversion results are shown in Figure 7. This example took

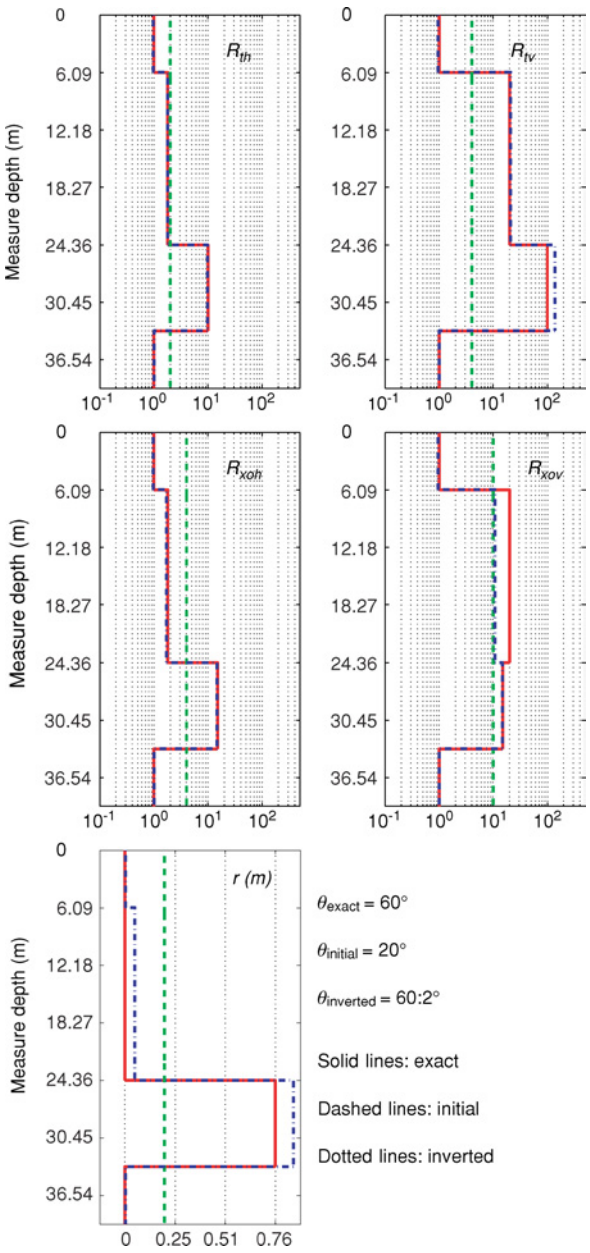

Figure 6. The inversion results of the dipping-bed model given in Figure 3 using data with 5% random white noise collected at 29 logging points.

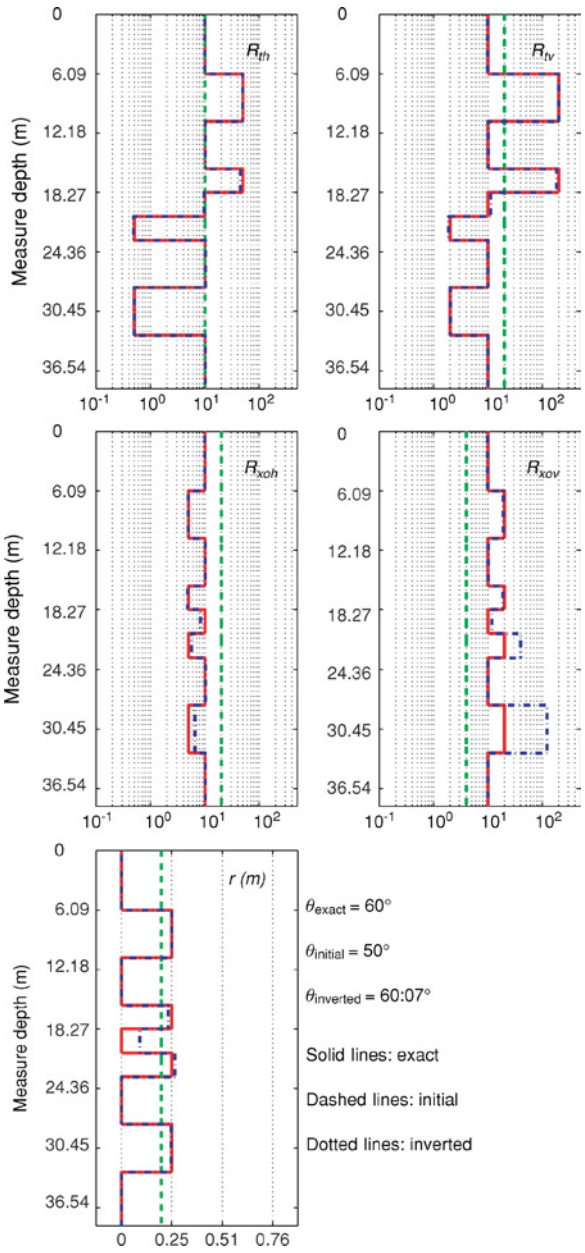

Figure 7. The inversion results of the nine-layer dipping-bed model using data with 5% random white noise collected at 69 logging points.

Table 2. Model parameters of the nine layer formation with dip and invasion; z_1 = 3.045 m and θ = 60°.

Δz (tvd in m)	R_{th} (Ω-m)	R_{tv} (Ω-m)	R_{xoh} (Ω-m)	R_{xov} (Ω-m)	r_i (m)
∞	10	10	10	10	0
2.436	50	200	5	20	0.254
2.436	10	10	10	10	0
1.218	50	200	5	20	0.254
1.218	10	10	10	10	0
1.218	0.5	2	5	20	0.254
2.436	10	10	10	10	0
2.436	0.5	2	5	20	0.254
∞	10	10	10	10	0

approximately 30 hours on a single PC with a Pentium IV 2.4-GHz processor. A parallelized version of the code is currently being implemented; it will reduce the inversion time to minutes instead of hours.

Finally, note that although this work is at a fairly early stage of its development, it clearly demonstrates the power of multicomponent, multispacing induction logging measurements in providing a robust inversion of formation parameters.

CONCLUSIONS

We developed one of the first full 3D parametric inversion algorithms devoted for the quantitative interpretation of multicomponent, multispacing induction logging measurements. By calculating the Jacobian matrix over a coarse finite-difference grid using the minimum-sized optimal grid, we can obtain the solution within acceptable computation time. Furthermore, by using the multiplicative regularization analysis, we can arrive at a robust parametric inversion scheme. Moreover, our study indicates that the triaxial induction tool has sufficient sensitivities to invert for both geometrical parameters as well as the material properties of the formation.

Future work will be directed toward studying the performance of the inversion algorithm to real field data.

ACKNOWLEDGMENT

The authors thank Tom Barber for providing an induction logging TI-anisotropic inversion example derived from a measured log in a field in Egypt.

REFERENCES

Abubakar, A., P. M. van den Berg, and S.Y. Semenov, 2003, Two- and three-dimensional algorithms for microwave imaging and inverse scattering: Journal of Electromagnetic Waves and Applications, **17**, 209–231.

Barber, T., B. Anderson, A. Abubakar, T. Broussard, K. C. Chen, S. Davydycheva, V. Druskin, T. Habashy, D. Homan, G. Minerbo, et al., 2004, Determining formation resistivity anisotropy in the presence of invasion: Annual Technical Conference and Exhibition, Society of Petroleum Engineers, paper 90526.

Davydycheva, S., V. Druskin, and T. M. Habashy, 2003, An efficient finite-difference scheme for electromagnetic logging in 3D anisotropic inhomogeneous media: Geophysics, **68**, 1525–1536.

Dennis, J. E., and R. B. Schnabel, 1983, Numerical methods for unconstrained optimization and nonlinear equations: Prentice-Hall Inc.

Druskin, V., and L. Knizhnerman, 1999, Gaussian spectral rules for the three-point second differences: I — A two-point positive definite problem in a semi-infinite domain: SIAM Journal on Numerical Analysis, **37**, 403–422.

Habashy, T. M., and A. Abubakar, 2004, A general framework for constraint minimization for the inversion of electromagnetic measurements: Progress in Electromagnetic Research, **46**, 265–312.

Kriegshauser, B., O. Fanini, S. Forgang, G. Itskovich, M. Rabinovich, L. Tabarovsky, L. Yu, M. Epov, P. Gupta, and J. van der Horst, 2000, A new multi-component induction logging tool to resolve anisotropic formations: 40th Annual Symposium, Society of Professional Well-Log Analysts, Transactions, paper D.

Kriegshauser, B., S. McWilliams, O. Fanini, and L. Yu, 2001, An efficient and accurate pseudo 2-D inversion scheme for multicomponent induction log data: 71st Annual International Meeting, SEG, Expanded Abstracts, 369–372.

Lu, X., and D. Alumbaugh, 2001, One-dimensional inversion of three-component induction logging in anisotropic media: 71st Annual International Meeting, SEG, Expanded Abstracts, 376–380.

Press, W. H., S. A. Teukol, W. T. Vetterling, and B. P. Flannery, 1992, Numerical recipes in FORTRAN: Cambridge University Press.

Rosthal, R., T. Barber, S. Bonner, K. C. Chen, S. Davydycheva, G. Hazen, D. Homan, C. Kibbe, G. Minerbo, R. Schlein, et al., 2003, Field test result of an experimentally fully-triaxial induction tool: 44th Annual Symposium, Society of Professional Well-Log Analysts, Transactions, paper O.

van den Berg, P. M., A. Abubakar, and J. T. Fokkema, 2003, Multiplicative regularization for contrast profile inversion: Radio Science, **38**, 23.1–23.10.

Wang, H., T. Barber, R. Rosthal, J. Tabanou, B. Anderson, and T. M. Habashy, 2003, Fast and rigorous inversion of triaxial induction logging data to determine formation resistivity anisotropy, bed boundary position, relative dip and azimuth angles: 73rd Annual International Meeting, SEG, Expanded Abstracts, 514–517.

Yu, L., B. Kriegshauser, O. Fanini, and J. Xiao, 2001, A fast inversion method for multicomponent induction log data: 71st Annual International Meeting, SEG, Expanded Abstracts, 361–364.

Zhang, Z., and A. Mezzatesta, 2001, 2D anisotropic inversion of multicomponent induction logging data: 71st Annual International Meeting, SEG, Expanded Abstracts, 365–368.

Zhang, Z., L. Yu, B. Kriegshauser, and L. Tabarovsky, 2004, Determination of relative angles and anisotropic resistivity using multicomponent induction logging data: Geophysics, **69**, 898–908.